Article:

Zongyou, Z., Nimmo, W., Cai, C. et al. (2026) Ultra-low-cut-in galloping of a reverse-C-with-tail piezoelectric harvester for low-speed wind energy conversion. Sustainable Energy Technologies and Assessments, 92. 105244. ISSN: 2213-1388

https://doi.org/10.1016/j.seta.2026.105244

Ultra-Low-Cut-In Galloping of a Reverse-C-with-Tail Piezoelectric Harvester for Low-Speed Wind Energy Conversion

Zuo Zongyou[a,b,*], William Nimmo[b], Chang Cai[a], Qingan Li[a], Ning Jia[a], Xiangyu Sun[a,*]

[a] National Energy Wind Turbine Blade R&D Center, Institute of Engineering Thermophysics, Chinese Academy of Sciences, Beijing 100190, China

[b] University of Sheffield, Sheffield S10 2GD, The United Kingdom

[*] Corresponding author: Zongyou Zuo, Email: zuozongyou@iet.cn. Xiangyu Sun, Email: sunxiangyu@iet.cn

These authors contributed equally as co-corresponding authors.

Supplementary Material

2. Harvester Design and Methodology

Table S1. Wind tunnel parameters.

Wind Tunnel Parameters	Specification
Maximum velocity	12 m/s or 500 rpm
Contraction ratio	6:1
Turbulence intensity	0.5% (can be increased if required)
Reynolds number per metre	1,200,000
Unsteady gust generation	±15% at 10 m/s and 2 Hz
Fan diameter	1,850 mm
Volume flow rate	31.1 m^3/s
Pressure	505 Pa
Fan absolute power	27.2 kW

3. Preliminary CFD Analysis and Aerodynamic Interpretation

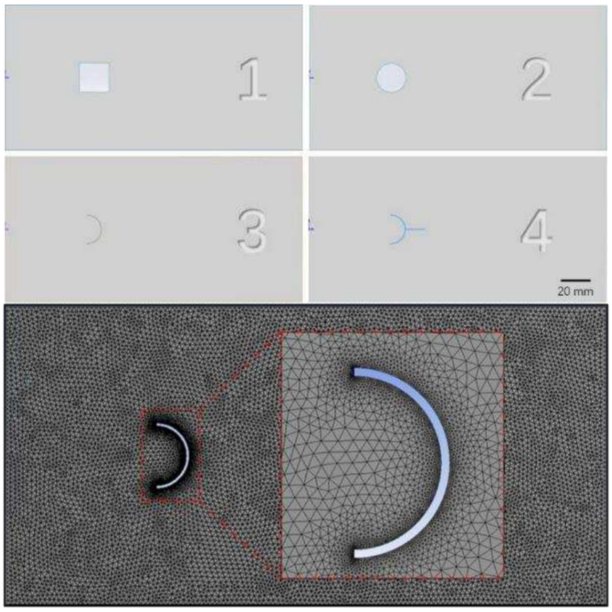

Figure S1. Two-dimensional computational domain (200 cm × 100 cm) and placement of the bluff-body models used in the preliminary CFD study.

Table S2. Summary of CFD setup and available quantitative metrics.

Item	Setting
Mesh type	Triangular mesh with local refinement near bluff body and tail
Mesh quality, S0	Element quality 0.964; aspect ratio 1.197; skewness 0.054; orthogonal quality 0.966
Mesh independence	Five meshes tested; variation in peak C_L < 5% after approximately 22652 elements
Extracted quantities	Lift-coefficient history, peak lift trend, response time, dominant frequency from C_L oscillation, vector/pressure/streamline fields
Non-extracted quantities	Pressure difference, recirculation length and vortex shedding frequency were not extracted as independent scalar metrics

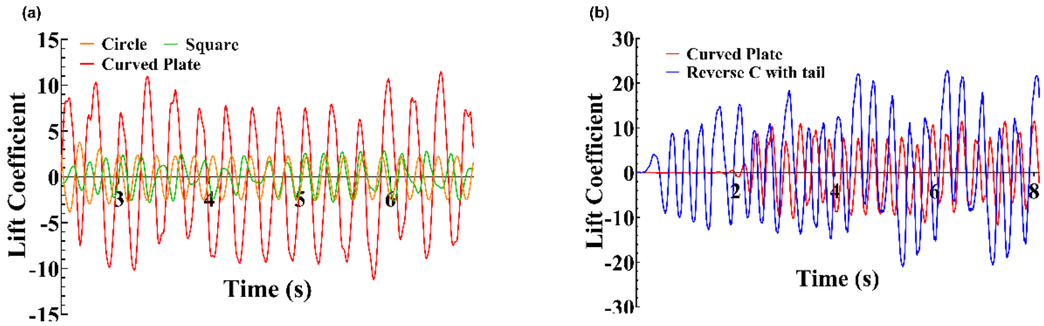

Figure S2. Comparison of lift-coefficient responses at 4 m/s for representative bluff-body geometries: **(a)** circular, square, and curved-plate sections; **(b)** curved-plate and reverse-C-with-tail configurations.

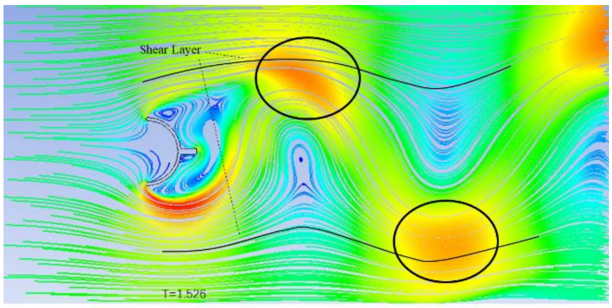

Figure S3. Velocity streamline diagram of the S1 model at lift coefficient peak (t=1.526 s), illustrating vortex formation and boundary layer interaction.

4. Experimental Results and Discussion

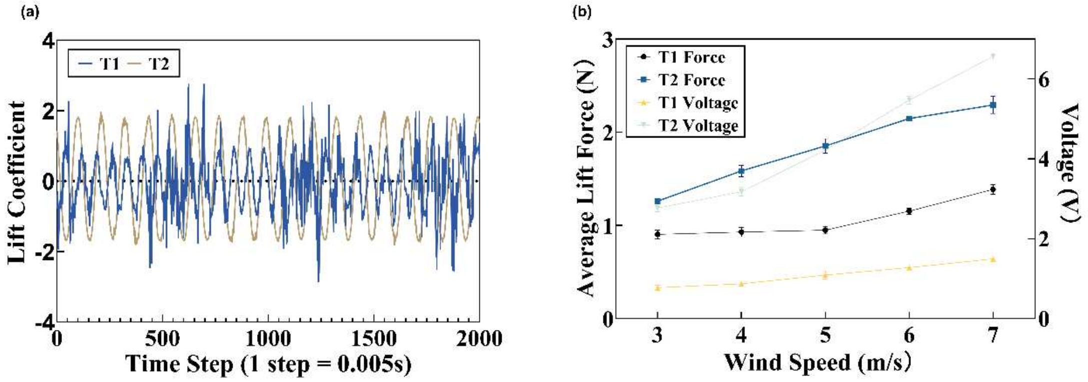

Figure S4. Effect of tail addition in the T-series: **(a)** lift-force histories of T1 and T2 at 5 m/s; **(b)** comparison of peak lift force and RMS voltage over the tested wind-speed range. Error bars represent standard deviations from repeated measurements.

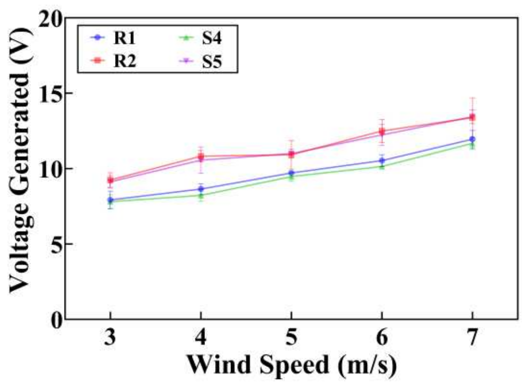

Figure S5. Voltage output comparison between R-series (R1, R2) and corresponding S-series (S4, S5) models over the tested wind-speed range. Error bars represent standard deviations from repeated measurements.

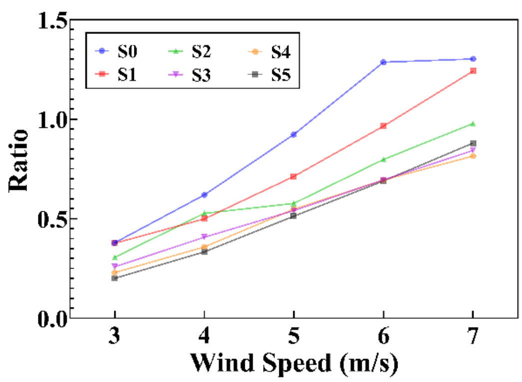

Figure S6. Ratio of experimentally measured lift force to CFD-predicted lift force for the S-series models over the investigated wind-speed range.

5. Reduced-Order Modelling and Trend Interpretation

Table S3. Key physical and structural parameters used in the reduced-order model.

Parameter	Symbol	Value
Natural frequency	f_n	9.5 Hz
Mechanical damping ratio	ζ_m	0.0025
Piezoelectric capacitance	C_e	15.1×10^{-9} F
Electromechanical coupling coefficient	Θ	0.51×10^{-4} N/V
Effective mass	M	0.023–0.047 kg
Linear stiffness	k	87–194 N/m
Damping coefficient	C	0.007–0.016 N·s/m

Table S4. Fitted aerodynamic coefficients A_1 and A_3 for the S-series models.

	S0	S1	S2	S3	S4	S5
A_1	1.01	1.57	2.39	3.30	4.94	6.41
A_3	859.93	279.38	291.31	262.93	272.69	241.10

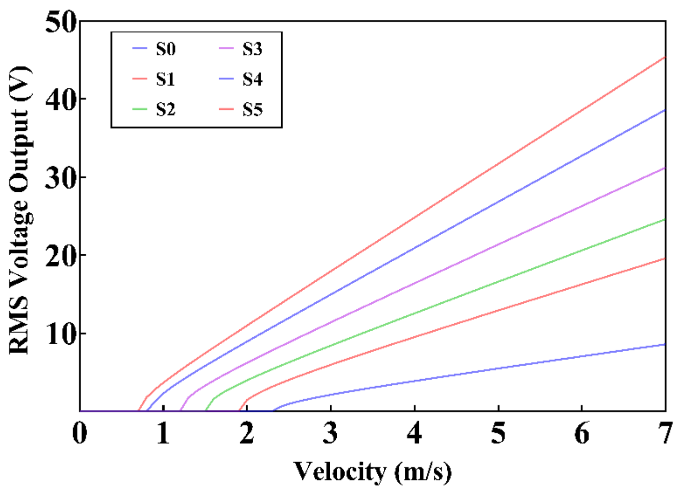

Figure S7. Modelled RMS-voltage trends for the S-series models obtained from the reduced-order electromechanical model after coefficient identification.